Evaluation of Hybrid Control and Palpation Assistance for Situational Awareness in Telemanipulated Task Execution

Rashid Yasin, Preetham Chalasani, Nicolas Zevallos, Mahya Shahbazi, Zhaoshuo Li, Anton Deguet, Peter Kazanzides, Howie Choset, Russell H Taylor, Nabil Simaan

***Abstract*—The use of intelligent feedback modalities to control and react to interaction forces during surgical procedures is an important factor in enabling safe and precise surgery. We explore the use of a model-mediated telemanipulation framework to enhance a user's situational awareness using assistive virtual fixtures and semi-automated task execution for safe and intuitive environment interaction during robotic laparoscopic surgery. The framework allows stiffness mapping with semi-autonomous excitation, hybrid position-force control, and model updates during soft geometry contact. A 24-person study was carried out at 3 sites in simulated ablation and palpation of phantom anatomy. Compared to methods lacking intelligent feedback and guidance, the proposed framework improved task execution metrics (force regulation, completion time, path-following error) and reduced user effort.**

***Index Terms*—model-mediated telemanipulation, surgical robotics, virtual fixtures, situational awareness, haptics**

I. Introduction

The introduction of robotics to minimally invasive surgery has enabled to use of dexterous manipulation tools with ergonomical controls for precise manipulation. However, robotic tools have disrupted the natural sensory feedback available to surgeons during manual open surgery. Complex interactions that can occur seamlessly during manual open surgery (e.g. digital palpation, organ retraction, and force-controlled ablation) are difficult during robot-assisted minimally invasive surgery (RAMIS) due to this sensory disruption.

To address this deficit, methods for giving surgeons greater sensory presence have included direct force feedback [1], sensory substitution [2]–[5], and virtual/augmented reality [6], [7] in applications such as force regulation in knot-tying [1], blunt dissection, [8] or palpation and environment stiffness exploration [6], [9]–[11]. However, there are limited works that have explored shared control with an autonomous agent during RAMIS [12], [13], motivating this paper's investigation into user assistance and partial autonomy.

Emerging surgical approaches such as single port access surgery and natural orifice endoscopic transluminal surgery are driving the need for complex high-degree-of-freedom robotic systems that operate under strict manipulation and perception constraints [14]. Such systems challenge existing approaches for haptic feedback due to manipulator-master asymmetry and because these robots are expected to enable complex interaction with the anatomy despite severe perception barriers. Given the amount of information needed to be interpreted, direct force feedback using a bilateral telemanipulation scheme cannot convey all the information required to the surgeon and more sophisticated approaches are needed. To address this need, we have put forth the concept of *Complementary Situational Awareness* (*CSA*) which uses a High-Level Controller (HLC) to update a virtual environment model using *in-vivo* sensory cues in order to provide assistance in certain aspects of robot-environment interaction while allowing surgeons to retain control over other aspects of the task[14], [15]. For example, using the CSA framework, a robot can use *in-vivo* palpation information to offer an update of the geometry of a virtual fixture (VF) in the presence of organ shift and deformation or perform guided stiffness exploration [16]–[19].

The ability of the CSA framework to map stiffnesses across the surface of an organ when palpating can augment surgeons' perception and allow them to localize and delineate boundaries of subsurface disease/anatomy like tumors or arteries. Incorporating stiffness information alongside geometric information can also improve the registration of pre-operative imaging to the intraoperative scene in RAMIS [16].

Previous works to estimate intraoperative stiffness information have traditionally required either specialized instrumentation or offline processing after the tissue has been probed or scanned. Approaches have included mechanical imaging [20], tactile arrays [21]–[24], robotic probing [10], [25]–[27] and tissue excitation for mechanical impedance estimation [28]. While there have been some initial results in e.g. visual tracking of applied forces during organ manipulation [29], there is a need for approaches that allow a user to understand organ stiffness without additional hardware or effort in performing palpation motion and interpreting visual or motion cues during robot-organ interaction.

To allow semi-autonomous behaviors and improve stability, the CSA framework uses model-mediated telemanipulation where control is mediated through a virtual environment model. In this framework, one challenge is that mismatched contact states can occur between the virtual model and the physical robot. Previous methods have updated the surface

R. Yasin, N. Simaan are with the Department of Mechanical Engineering, Vanderbilt University, Nashville, TN 37235, USA. e-mail: (rashid.m.yasin, nabil.simaan)@vanderbilt.edu.

P. Chalasani, M. Shahbazi, Z. Li, A. Deguet, P. Kazanzides, R. H. Taylor are with the Department of Computer Science, Johns Hopkins University, Baltimore, MD 21218, USA. e-mail: (pchalas1, mahya.sh, maxwell.li, anton.deguet, pkaz, rht)@jhu.edu

N. Zevallos, H. Choset are with the Robotics Institute at Carnegie Mellon University, Pittsburgh, PA 15213, USA. e-mail: (nzevallo, choset)@cmu.edu

location for interaction in a single direction [30], [31] or the orientation of a constraint frame during cutting operations in satellite servicing tasks [32] , however none have explored updates during contact with curved geometry. When using model-mediation and hybrid control, as in [33], updates to the virtual contact state have to be performed carefully to avoid discontinuities in the forces applied to the user's hand especially in the presence of non-planar geometry.

This paper reports evaluation of several assistive approaches in the context of model-mediated telemanipulation for force regulation and force-guided exploration. In regulation, we use semi-autonomous force control alongside VFs for force-controlled mock ablation along a path. In exploration, we use assistive palpation and stiffness mapping methods to enable the detection of mock tumors embedded in phantom anatomy. We hypothesize that assistive feedback and semi-autonomous control can limit cognitive load and improve user performance. We design an evaluation study that compares our assistive framework to standard telemanipulation approaches.

The work reported in this paper builds on our prior work where a framework for continuous palpation and assistive telemanipulation has been presented [34], [35]. We claim three contributions in expanding the utility of this framework. First, we present a low-frequency positional update of the virtual model in order to reconcile virtual and measured robot positions during long periods of interaction with a curved environment. Second, we define VF laws and semi-autonomous behaviors to assist a user during force-regulated task completion and exploratory palpation. Third, we explore the utility of semi-automated palpation to assist in the identification of stiff subsurface features.

The remainder of this paper is organized as follows: Section II describes the robot control architecture and implementation of the model-mediated telemanipulation structure, along with the stiffness estimation algorithms and visual feedback assistance modes for users. Section III presents the experimental setup for a user study of mock ablation and palpation, the details of which are described in section IV. We then summarize the results of the user study in section V and present a discussion and concluding remarks in sections VI and VII. Table I lists the terminology used in this paper.

TABLE I: Table of Terminology

Term	Description
RAMIS	Robot-Assisted Miminally Invasive Surgery
HLC	High-Level Controller
MTM	Master Tool Manipulator (master device)
PSM	Patient-Side Manipulator (slave device)
VF	Virtual Fixture
PVF	Positional Virtual Fixture
OVF	Orientational Virtual Fixture
FRMM	Force-Regulated Model-Mediated Telemanipulation
$\mathbf{p}, \widetilde{\mathbf{p}}$	Robot position, virtual "proxy" robot position
$\mathbf{c}, \mathbf{s}$	Closest point to the robot on a curve, on a surface
$\tilde{\mathbf{c}}, \widetilde{\mathbf{s}}$	Closest point to the proxy on a curve, on a surface

II. System Control Architecture

We evaluated our methods on the da Vinci Research Kit (dVRK) [36], [37] utilizing the Johns Hopkins University "Surgical Assistant Workstation (SAW)" software environment [38] in a Linux environment. The users controlled one dVRK Patient Side Manipulator (PSM) to interact with a phantom organ model of a kidney by grasping the right arm of the dVRK Master Tool Manipulator (MTM) with a stereo viewer to provide visual feedback.

The control architecture follows that presented in [34], with updates to VF definitions and model update techniques. The general framework is shown in Fig. 1. The HLC is responsible for the type of telemanipulation connection between the MTM and PSM and uses a number of sub-components: telemanipulation feedback modes; model updates to account for differences between the environment model and the real robot; an orientational VF; a positional VF; and stiffness estimation using gaussian processes. Telemanipulation motion scaling is applied in all modes with a $\frac{2}{5}$ positional scaling to increase positional accuracy and a one-to-one orientational scaling for intuitive control.

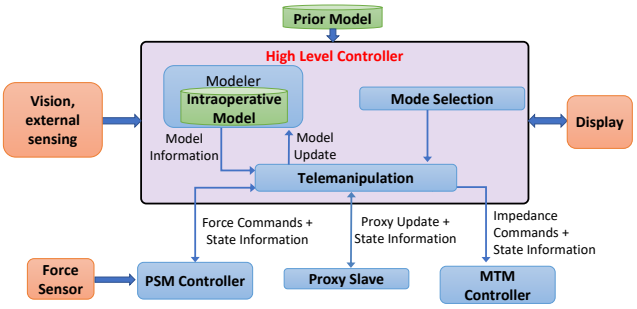

Fig. 1: Control diagram of the CSA framework, figure adapted from [34].

A. High-Level Telemanipulation Feedback Modes

The HLC was designed to allow three control/feedback modes for robot-environment interaction: unilateral telemanipulation, bilateral telemanipulation, and force-regulated model-mediated telemanipulation (FRMM).

In unilateral telemanipulation, the controller does not have any knowledge of the environment geometry or robot-environment interaction forces. This mode is similar to that of current commercial systems that have no force sensing or force feedback. Velocity commands from the MTM are directly sent to the PSM resulting in pure position control. No forces are felt by the user at the MTM, which uses the gravity compensation method of [39], but no other active control. The only safety feature is in the low-level control of the PSM, which turns off the motors if a high current or tracking error are detected.

In bilateral telemanipulation, the MTM operates under force control, directly sending the measured PSM-environment forces to the MTM handle. To reduce oscillatory behavior due to time delays between robot controller and the force sensor data acquisition hardware, the forces were scaled with a gain of 0.75 before being sent to the MTM. Like unilateral telemanipulation, velocity commands of the MTM are sent to the PSM, which operates in position control.

In FRMM, a model-mediated framework allows independent PSM-organ interaction and MTM feedback. The user's

hand movements control the position of a "proxy PSM", which interacts with a virtual model of the environment [34]. The interaction between the virtual environment and the proxy PSM generates the forces sent to the MTM using an *a-priori* environment model in the form of a triangular mesh with an assigned stiffness normal to the surface.

When the proxy PSM is above the model surface, the MTM controls the position of the proxy PSM, which directly updates the PSM position reference - mimicking unilateral telemanipulation. When in contact, an indirect hybrid position-force controller regulates forces on the PSM, independent of the proxy, following established methods as in [40], [41]. At any given location of the proxy PSM, the local surface normal $\hat{\mathbf{n}}$ is calculated from model and used to calculate two projection matrices for the force and position controllers, $\mathbf{\Omega}_f$ and $\mathbf{\Omega}_p$, such that:

$$\mathbf{\Omega}_f = \hat{\mathbf{n}}\hat{\mathbf{n}}^{\mathrm{T}}, \quad \mathbf{\Omega}_p = \mathbf{I}_3 - \hat{\mathbf{n}}\hat{\mathbf{n}}^{\mathrm{T}} \tag{1}$$

where $\mathbf{I}_3 \in \mathbb{R}^{3\times3}$ is the identity matrix. At each control time step, the desired PSM velocity, $\dot{\mathbf{p}}$, is calculated as:

$$\dot{\mathbf{p}} = \mathbf{\Omega}_p\dot{\widetilde{\mathbf{p}}} + \mathbf{\Omega}_f\mathbf{K}_f(\mathbf{f}_{ref} - \mathbf{f}_{cur}) \tag{2}$$

and input into a resolved-rates algorithm to produce a joint position reference to a PD joint position controller. The first term $\mathbf{\Omega}_p\dot{\widetilde{\mathbf{p}}}$ takes into account the current velocity of the proxy PSM $\dot{\widetilde{\mathbf{p}}}$ and produces a velocity command in the local tangent plane of the environment model. The second term $\mathbf{\Omega}_f\mathbf{K}_f(\mathbf{f}_{ref} - \mathbf{f}_{cur})$ uses an admittance gain $\mathbf{K}_f$ to produce a velocity command in the direction normal to the surface of the local environment model using the current and desired forces on the robot, $\mathbf{f}_{cur}$ and $\mathbf{f}_{ref}$.

The model-mediated framework allows assistive actions without disrupting the user. While the user retains control over the lateral motion of the MTM and feels intuitive feedback through interaction with the model environment, the PSM maintains independent force control. This enables high-performance force regulation while retaining intuitive user control.

B. Contact State Mismatch Between the Proxy and Real PSM

When using FRMM telemanipulation, the contact state of the real PSM with the environment and the contact state of the proxy PSM with the model environment may develop a mismatch. Real contact is detected when interaction forces exceed 0.1N, and proxy contact when the proxy intersects the environment mesh. A set of scenarios must be accounted for:

- When both the PSM and the proxy PSM are in contact, the hybrid position-force controller is engaged.
- If neither are in contact, the MTM motion controls the position of the proxy PSM in unilateral telemanipulation, directly updating the position reference for the PSM.
- If only the proxy is in contact, the hybrid position-force control is engaged to push the PSM onto the surface. This assumes that registration errors are small; model updates could be used to reduce errors if required [31].
- If only the PSM is in contact, the hybrid position-force control is engaged to prevent the user from imparting unsafe forces to the surface without noticing (since no forces will be reflected on the MTM as long as the proxy PSM is not in contact with the environment model).

In order to allow the user to leave the surface, there must be a way to turn off the hybrid position-force controller as the user commands motions off of the organ. Therefore, when the PSM is in contact, but the proxy is more than 2mm away from the organ, the hybrid position-force controller is disengaged and unilateral telemanipulation is engaged as long as the PSM is moving away from the organ or until the proxy comes within the 2mm band again. This 2mm threshold was determined based on the experimentally characterized average fiducial localization error of approximately 1.0 mm when using the PSM as a digitizer [42], [43]. This maintains safe and intuitive control while still allowing users to leave and enter contact smoothly.

Algorithm 1 shows the control mode selection based on the contact states. $\widetilde{\mathbf{p}}$ denotes the proxy PSM position and $\widetilde{\mathbf{s}}$ the closest point on the environment model to the proxy PSM.

Algorithm 1 Contact State Control Modes

```
Mode Selection:
if (Proxy Contact) then
    Hybrid position-force control          ▷ Full Contact or Proxy Contact
else (Proxy in Freespace)
    if (Slave Contact) then
        if (||p̃ − s̃|| > 2mm & ṗ̃ · n̂ > 0) then
            Position control                          ▷ Leaving Slave Contact
        else
            Hybrid position-force control             ▷ Slave Contact
        end if
    else
        Position control                              ▷ No Contact
    end if
end if
```

C. Position Discrepancy Between the Proxy and Real PSM

When using the hybrid controller, the filtering of position commands by $\mathbf{\Omega}_p$ and independent motions from the force controller can lead to positional discrepancies between the proxy and real PSM after prolonged interaction. If this discrepancy is not rectified, forces felt on the MTM (based on the current position of the proxy PSM) may be substantially different in magnitude and direction relative to those experienced by the PSM (caused by environment interaction). These erroneous forces can confuse the user and cause undesirable motion. Therefore, the proxy PSM position must be updated to match that of the PSM.

If the HLC instantaneously updates the position of the proxy PSM to the current PSM position, the model-mediated nature of the controller is compromised. For example, if the interaction force between the proxy PSM and the model environment is larger than that of the PSM on the real environment, the position update will place the proxy PSM higher than it was before the update. The user, trying to regulate forces, will feel a decrease in the force feedback, and will push down again. However, the next update will again replace the proxy PSM higher, effectively resulting in users feeling like they can "fall through" the model environment. Therefore, a simple continuous update should be avoided.

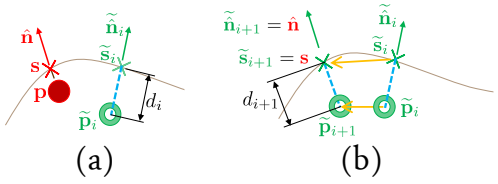

Fig. 2: Achieving a haptically continuous proxy PSM update: (a) proxy and real PSM discrepancy before the update, (b) proxy PSM position update.

A more complete update strategy is shown in Fig. 2 which allows model interaction while also preserving *haptic continuity*, i.e., no jumps in the MTM interaction forces during nominal operation. In Fig. 2a, the current position of the PSM, its local surface normal and closest point to the model surface are represented as $\mathbf{p}$, $\hat{\mathbf{n}}$, and $\mathbf{s}$, respectively. The current position of the proxy PSM, $\widetilde{\mathbf{p}}_i$ corresponds to a closest point $\widetilde{\mathbf{s}}_i$ on the model surface, with a penetration depth d_i along the local surface normal $\widetilde{\mathbf{n}}_i$. In Fig. 2b, the updated proxy PSM position, $\widetilde{\mathbf{p}}_{i+1}$, is given by:

$$\widetilde{\mathbf{p}}_{i+1} = \mathbf{s} - d_{i+1}\hat{\mathbf{n}} \tag{3}$$

Assuming that location $\widetilde{\mathbf{s}}_i$ has an associated normal stiffness k_i then the magnitude of the force calculated by the model is $f_i = k_i d_i$. After the proxy update, the magnitude of this force should be constant, i.e. $f_{i+1} = f_i$. Therefore, assuming the normal stiffness at location $\mathbf{s}$ is k_{i+1}, then the penetration depth, d_{i+1}, should be:

$$d_{i+1} = \frac{d_i k_i}{k_{i+1}} \tag{4}$$

In in this study, the environment had a constant stiffness, so $d_{i+1} = d_i$. This resolves the issue of keeping a constant force magnitude during the update. For the general case of a probe moving across a surface with minimum local curvature ρ at some maximum velocity v_{max}, the maximal angular disturbance $\delta\theta_{max}$ (change in direction between $\hat{\mathbf{n}}_i$ and $\hat{\mathbf{n}}_{i+1}$) caused by an update running with a period of δt will be:

$$\delta\theta_{max} \approx \frac{v_{max}\delta t}{\rho} \tag{5}$$

This shows that if the position discrepancy update is run slowly, the user moves very quickly, or the surface has sudden changes in surface normal, the update will introduce discernable haptic discontinuity as the update changes the direction of forces on the MTM.

The update cycle time δt can be reduced to maintain fidelity of proxy and real PSM positions. However this cycle time should be significantly larger than the telemanipulation cycle time of the HLC to avoid having the repetitive updates conflict with intended motions of the user. In the experiments below using an environment model without surface discontinuities, an HLC telemanipulation loop frequency of 200 Hz, and a position discrepancy update frequency of 1 Hz, the update was not noticeable to the users.

D. Orientational Virtual Fixture

Large pitch angles of the PSM end-effector are not ideal for forceful interaction, as they can cause large torques on the instrument wrist. To resolve this problem and to help the users in tasks of ablation and palpation, we applied an orientational VF (OVF) to the MTM (whose orientation in the dVRK control framework always matches that of the PSM). The desired orientation for the OVF was derived from the environment local surface normal at the point closest to the PSM end effector. The user was free to rotate the tool about the local surface normal, but a nonlinear stiffness prevented the axis of the tool from deviating far from the local normal.

To calculate the torques applied on the MTM wrist by the OVF, we defined a frame $\{\mathrm{s}\}$ having is z axis aligned with the local environment surface normal at the point closest to the PSM tip and its x axis parallel to that of the PSM end effector frame $\{\mathrm{p}\}$. Denoting the orientation of this frame as $\mathbf{R}_s$ and the orientation of the PSM wrist as $\mathbf{R}_p$, the torque applied to the MTM, $\boldsymbol{\tau}_{vf}$, was calculated as:

$$\boldsymbol{\tau}_{vf} = \mathbf{K}_\theta \hat{\mathbf{m}} \theta_e^2 \tag{6}$$

$$\theta_e = \cos^{-1}\left(\frac{tr(\mathbf{R}_s^{\mathrm{T}}\mathbf{R}_p) - 1}{2}\right) \tag{7}$$

$$\hat{\mathbf{m}} = \frac{[(\mathbf{R}_s^{\mathrm{T}}\mathbf{R}_p) - (\mathbf{R}_s^{\mathrm{T}}\mathbf{R}_p)^{\mathrm{T}}]^\vee}{2\sin(\theta_e)} \tag{8}$$

$$\mathbf{K}_\theta = diag(k_\theta, k_\theta, 0) \tag{9}$$

where $\hat{\mathbf{m}}$ and θ_e are the axis-angle parametrization of the orientation error of $\{\mathrm{s}\}$ relative to $\{\mathrm{p}\}$. The operators $[*]^\vee$, $tr(*)$, and $diag(*)$ extract the vector from a skew-symmetric matrix, compute the trace of a matrix, and make a diagonal matrix with the elements of $*$ on the main diagonal, respectively.

When the user is far from the surface, the closest point on the environment may jump between different locations and introduce discontinuities in $\mathbf{R}_s$. To maintain haptic continuity, an interpolated frame $\{\mathrm{i}\}$ was used in place of $\{\mathrm{s}\}$ in the above equations. $\mathbf{R}_i$ was initialized equal to $\mathbf{R}_s$ and constantly moved toward $\mathbf{R}_s$ using an axis-angle interpolation. A rotational error matrix $d\mathbf{R}$ was calculated using the interpolated rotation at the previous timestep, $\mathbf{R}_{i-1}$

$$d\mathbf{R} = \mathbf{R}_{i-1}^{\mathrm{T}}\mathbf{R}_s \tag{10}$$

Using (7) and (8), $d\mathbf{R}$ was broken down into its axis-angle representation with axis $\hat{\boldsymbol{\omega}}$ and angle γ. These components were used to rotate the current orientation $\mathbf{R}_i$ toward $\mathbf{R}_s$ by k_i radians per time-step.

$$\mathbf{R}_i = \begin{cases} \mathbf{R}_s, & \text{if } \gamma < 0.01 \\ \mathbf{R}_{i-1}e^{k_i\hat{\boldsymbol{\omega}}} & \text{otherwise.} \end{cases} \tag{11}$$

This broadly aligned the VF with $\{\mathrm{s}\}$, but prevented sudden changes in $\mathbf{R}_s$ from causing large changes in $\boldsymbol{\tau}_{vf}$.

E. Positional Virtual Fixture

A positional virtual fixture (PVF) was used to guide the user's hand to follow some desired path on the surface of the environment. This was achieved through a soft barrier VF with a constant stiffness k_y that restricted movement transverse to the path on the MTM. A diagram of the PVF is shown in Fig. 3.

The PVF was calculated with the use of a compliance frame $\{\widetilde{c}\}$, located at the closest point, $\widetilde{\mathbf{c}}$, on the ablation path to the PSM tip. The x axis of $\widetilde{\mathbf{c}}$ was oriented along the local tangent of the ablation path, the z axis along the outward-pointing surface normal, and the y axis according to the right-hand rule. The force of the PVF was calculated in the PSM base frame, $\{\mathrm{b}\}$, using the equation:

$$\mathbf{f}_{vf} = \left({}^{\widetilde{c}}\mathbf{R}_b\right)^{-1} \mathbf{K}_p {}^{\widetilde{c}}\mathbf{R}_b(\widetilde{\mathbf{c}} - \widetilde{\mathbf{s}}) \tag{12}$$

$\widetilde{\mathbf{s}}$ is the point on the model environment surface that is closest to the proxy PSM. $\mathbf{K}_p$ is the VF stiffness gain matrix. The rotation ${}^{\widetilde{c}}\mathbf{R}_b$ rotates a vector in frame $\{\mathrm{b}\}$ to be represented in frame $\{\widetilde{c}\}$.

To prevent users from leaving the finite-length ablation path, a stiffness k_x was applied when the user was outside the finite length of the curve. Two planes were defined in the y-z plane of the VF compliance frame $\{\widetilde{c}\}$ at either end of the ablation path, Fig. 3. A point $\widetilde{\mathbf{s}}$ was determined to belong to the curve (i.e. $\widetilde{\mathbf{s}} \in curve$) if it was between these planes. The VF stiffness matrix was defined as:

$$\mathbf{K}_p = diag(k_x, k_y, 0) \tag{13}$$

$$k_x = \begin{cases} 0, & \text{if } \widetilde{\mathbf{s}} \in curve \\ k_y, & \text{otherwise.} \end{cases} \tag{14}$$

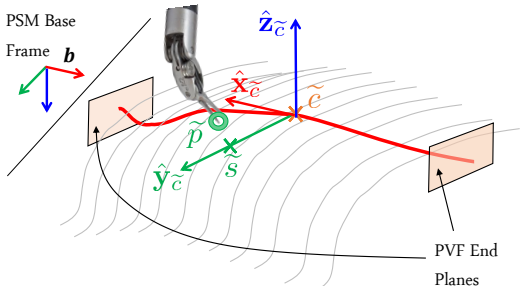

Fig. 3: Positional virtual fixture to push user's hand toward the closest point on the desired fixture curve.

F. Stiffness Estimation Using Gaussian Processes

As part of the *CSA* framework, a stiffness estimation module was included to semi-autonomously palpate the environment and create a stiffness map of the surface. Using the method of [35], a force-based sinusoidal palpation motion was superimposed over the user's movement commands during surface exploration. A force reference in Newtons was set into the controller in (2) as a sinusoid with amplitude A, bias B, and frequency h (in Hz):

$$\mathbf{f}_{ref} = A\sin(h\pi t) + B \tag{15}$$

The motion and force information collected during palpation were used to define a Gaussian Process model of the interaction force as a function of the probe location. Using this model, the local stiffness can be calculated along the palpation direction by dividing the force difference by the distance between deep and shallow interaction points. Surface locations are estimated by calculating the zero-intercept of a linear fit of the interaction forces as a function of the palpation positions in a given palpation cycle.

In order to increase computational efficiency, local Gaussian process models were used to estimate forces within different areas of the surface. Two spatial hash grids were defined: one for the training set data and another for prediction data. By fitting models to local areas of the stiffness map, greater computational efficiency was achieved for online stiffness estimation. Additionally, because Gaussian process regression is sensitive to redundant data points, the hashing process prevented excess data from corrupting the regression. Details of the method are available in [35].

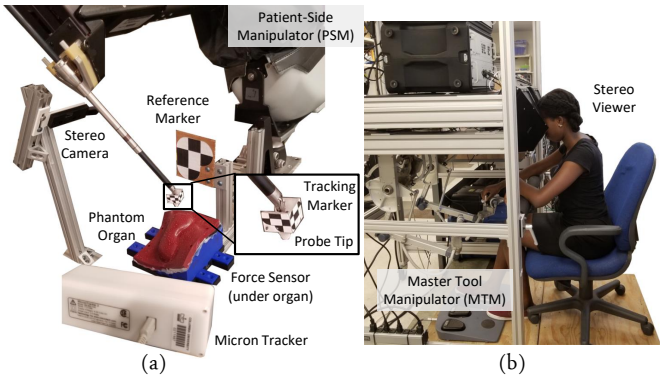

Fig. 4: (a) Experimental setup for a user study, replicated at 3 universities (b) User grasping the MTM while looking into the stereo viewer

III. Experimental Setup

The experimental setup is shown in Fig. 4. Alongside the dVRK system explained in section II, an eYs3D (Taipei, Taiwan) EX8029 stereo camera with a 3cm baseline captured images shown to the user through the stereo viewer in Fig. 4b. Depending on the site, either a Nano 17 or a Gamma 6-axis force sensor from ATI (Apex, North Carolina) was mounted below the phantom kidney and sampled at 1 kHz, as a stand-in for any of a number of force-sensing methods that could be integrated into a clinical system, as reviewed in [44], [45]. The PSM end-effector gripped a probe with a teflon sphere on its tip and optical tracking markers attached to the sides for position measurements using the Claron Technology (Ontario, Canada) MicronTracker 2 optical tracking system. The RMS tooltip tracking error was 0.7mm in position and 2.3° as determined from a Monte Carlo simulation based on the manufacturer-reported accuracy of 0.2mm for a given tracked point. Optical tracking was used for registration and positional measurements in post-processing of the experimental datanot in the real-time control loop.

A. Silicone Model Preparation

Two sets of silicone phantom organs were made for ablation and palpation tasks. The molding and mounting process can be seen in Fig. 5. Fig. 5c shows the phantom organs glued to a 3D-printed platform with digitization divots to consistently deform them from their "preoperative" state of the mold

geometry. The ablation phantoms were kept transparent and a red curved silicone rubber rod (durometer 40A) was set into the ablation phantoms to represent a desired ablation path. The palpation phantoms were made of the same silicone, but dyed red. A set of 2 or 3 hard teflon spheres were embedded below the surface where they could be felt, but not seen. Both phantoms measured approximately 7 inches per side.

To find the location of the stiff features, CT scans of the organs were taken using a Xoran xCAT® ENT scanner (Xoran Technologies, Ann Arbor, MI) with isotropic voxels resolution of 0.3mm. These scans were manually segmented using 3D Slicer [46] to find the ground truth subsurface path and sphere locations.

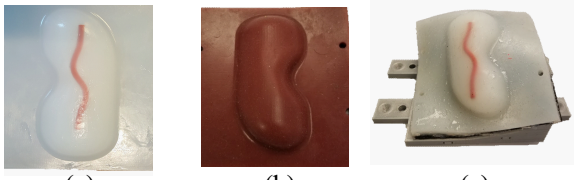

(a) (b) (c)

Fig. 5: Example phantom kidneys created from silicone with embedded stiff features: (a) Ablation phantom (b) Palpation phantom (C) Deformed phantom used in experiments, mounted to a base with digitization divots.

B. Organ and Stereo Registration

The use of a model-mediated controller requires an accurate model of the environment that is properly registered to the robot during telemanipulation. The registration between the MTM, PSM, and force sensor were calculated using a priori knowledge of the geometry of the experimental setup and the attachment of the force sensor to its mounting platform. The location of the 3D printed base with respect to robot frame was obtained by using the PSM to digitize the centers of the divots in 3D printed base. The locations of the divot centers and the embedded spheres were also obtained in CT frame through segmentation using 3D Slicer. Using a fiducial localization error of 1mm when using the PSM to digitize the divots [42], the expected average target registration error (TRE [47]) for the points along the ablation path was 0.8 mm.

Because the focus of this study was not on intraoperative registration, we used the CT scans of the deformed organs as seen in Fig. 5c as inputs into the coherent point drift deformable registration algorithm [48] to generate the in-experiment environment surface models. The geometry of the silicone mold was used as the "preoperative" model to create a unique model for each phantom. This assumes more information than would typically be available in a surgical scenario, but could be replaced with some visual mapping method or previous methods we have presented using palpation for intraoperative registration [16], [19], [49]. Such intraoperative registration steps were excluded to maintain a reasonably low experimental protocol duration and complexity.

A variety of image overlays were included in the experiment including a force bar that moves with the PSM tip and an STL model of the mock organ that was colored to display stiffness information obtained during palpation. To successfully achieve these overlays, the stereo camera was also registered to the robot frame. The spherical palpation tip attached to the PSM gripper shown in Fig. 4a was painted red and segmented using color segmentation. The stereo image to robot registration used paired-point rigid registration [50]. The point pairs were obtained by moving the PSM end-effector to a number of points in the robot workspace and collecting end-effector locations in robot frame and stereo frame. This registration was used directly for the force-bar overlay, but was not sufficiently accurate for the overlay of the model organ on the visible silicone phantom since small errors in registration orientation meant that portions of the overlay would intersect the real organ. This was overcome with manual adjustment of the model organ overlay to minimize user confusion.

	Unaided	**Visual**	**Bilateral**	**FRMM**
Control Mode	Unilateral	Unilateral	Bilateral	FRMM
OVF	On	On	On	On
PVF	Off	Off	On	On
Overlay	None	Force Bar	Force Bar	Force Bar

TABLE II: Assistance modes for mock ablation experiments.

IV. User Study

A multi-site user study was carried out to characterize the effect of different assistance modes on the mock execution of two basic surgical tasks: ablation and palpation. 26 individuals were enrolled in an Institutional Review Board-approved study. These participants were recruited from the graduate student populations at Vanderbilt, Johns Hopkins, and Carnegie Mellon Universities. Two users were removed from consideration due to data corruption, permitting a full analysis of 24 users. No users had prior robotic surgical experience, but the average experience with telemanipulated devices was a 2 on a scale of 1 to 4. The same hardware and software setup was replicated at each site to show the cross-compatibility of this software framework. An example runthrough of the user study can be found in Multimedia Extension I.

On arriving, after being consented, each user was given approximately 10 minutes to get familiarized with the system and how to use the robot. The user was then guided while carrying out the tasks in the following sections. After each section of the experiment, the user was asked to fill out a survey to subjectively evaluate their experience and the differences between the assistance modes.

In all modes, an OVF (section II-D) was applied to the user's wrist to assist in aligning the user with the local surface normal of the phantom organ. In preliminary experiments, inexperienced users often allowed the wrist to tilt very far from the surface normal unless assisted, so this assisted in maintaining proper probe orientation.

A. Mock Ablation Task

The mock ablation experiment consisted of following a visible path from one side of a silicone kidney phantom to the far side and back while maintaining a constant interaction force of 3 N. The path-following task was repeated for four different types of feedback modes as outlined in Table II. For

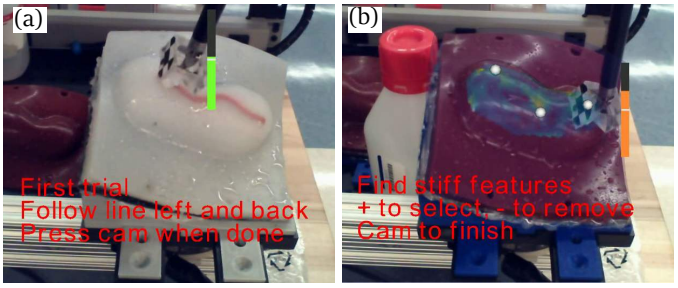

Fig. 6: (a) Image from stereo viewer of user view during an ablation experiment. Force feedback measurement shown in the vertical bar, overlay text assists in giving instructions to the user. (b) Augmented reality view during palpation experiment of stiffness map overlaid on top of an organ with points selected by the user displayed on the organ's surface.

each mode, the task was completed three times, consecutively.

In the first mode, termed the "Unaided" mode, the user relied only on visual feedback through the MTM stereo viewer (i.e. no force feedback). This mode is comparable to current capabilities of commercial robotic surgical systems. To train each user to apply a constant target ablation force, they were instructed to slowly press into a bulk region of the phantom organ (i.e. not above a stiff feature) until the desired force was reached. Visual feedback about the force was presented to the user only during this training phase and it consisted of a color bar overlay as shown in 6A. The bar changed in color from red to green to indicate level of force error. Pure green indicated the force was at the desired level and red indicated a force error was at or larger than 6N or close to 0N. After training with the color bar overlay, each user was asked to reach the target force without the bar's assistance. Before commencing the ablation experiments, each user was expected to repeat their training and validation with/without the color bar until they were able to reach the desired force of 3N at least 3 times out of a set of 5 consecutive attempts.

In the second "Visual" mode, the user still had no haptic assistance in completing the task, but were aided by the color overlay of ablation force. This visual force feedback was also present in all the subsequent modes.

In the third mode, the user operated using bilateral telemanipulation. In addition, a PVF was added to the MTM such that the user's hand was pushed to follow the shape of the desired curve. The bilateral telemanipulation provided direct force feedback on the master in order for the user to attempt to apply a consistent desired contact force in the normal direction of the organ surface under both kinesthetic feedback from the master and visual guidance using the force bar.

In the fourth mode, the user operated using FRMM alongside the same tangential alignment PVF as the previous mode. Using FRMM, the master interacted with a constant-stiffness virtual environment model while the PSM independently was under hybrid position-force control. This allowed the user to maintain control of the telemanipulation direction and when to make/leave contact, but severed the direct link between master and slave allowing the slave to independently control interaction forces to increase safety and improve force regulation.

	Bilateral	**FRMM + Overlay**
Control Mode	Bilateral	FRMM + Sinusoid
OVF	On	On
PVF	Off	Off
Overlay	Force Bar	Force Bar, Stiffness Map

TABLE III: Assistance modes for mock organ palpation experiments.

B. Organ Palpation Task

The second benchmark task was organ palpation to find hidden subsurface features. We therefore investigated the reliability and efficacy of detecting hidden subsurface features using robot-assisted telemanipulation.

The two feedback modes used for telemanipulated palpation are summarized in table III. In the first mode, the user had only direct force feedback through bilateral telemanipulation and they were also aided by the same colorbar overlay as in the ablation experiments.

In the second mode, "FRMM+Overlay" the same palpation task was carried out, but under FRMM control. The reference force was set as a sinusoid as in (15) with $A = 2$, $B = 2$, $h = 5$. The measured forces were not relayed back to the user directly and instead were fed into the GP stiffness mapping method presented in section II-F. This stiffness map was visually overlaid on top of the organ in the stereo viewer for the user to see where potential locations of high stiffness might exist. Users could at any time digitize the location of stiff features by pressing a footpedal. Digitized locations were overlaid with a sphere on the organ surface as shown in Fig. 6b.

For each mode, users attempted to find stiff subsurface features in 2 phantom organs, repeating each organ once, for a total of 4 trials per control mode. The order of organs was randomized for each user and the users were blinded to the order in which the organs were presented to them.

V. Results

A. Mock Ablation

The performance of users was evaluated based on the performance metrics shown in table IV. The key metrics were the lateral path following error calculate as the mean norm lateral error from the path, the mean force regulation error along the path, the average completion time for each back-and-forth pass over the ablation path, the path coverage, which is defined as the percentage of path length during which contact between the end-effector tip and the mock anatomy was registered by the force sensor. This metric was calculated by discretizing the desired path and calculating the closest segment for each position of the robot while in contact.

Refering to table IV for the mock ablation experimental results, it can be seen that the users were able to complete the task best in all metrics using the fourth mode under FRMM control. Statistical comparisons of metrics between the 4 groups was performed via Tukey's honest significant difference criterion using MATLAB's statistical toolbox. This gives an estimate for significant difference of the means between the 4 groups while accounting for the additional errors brought by testing differences among all the groups.

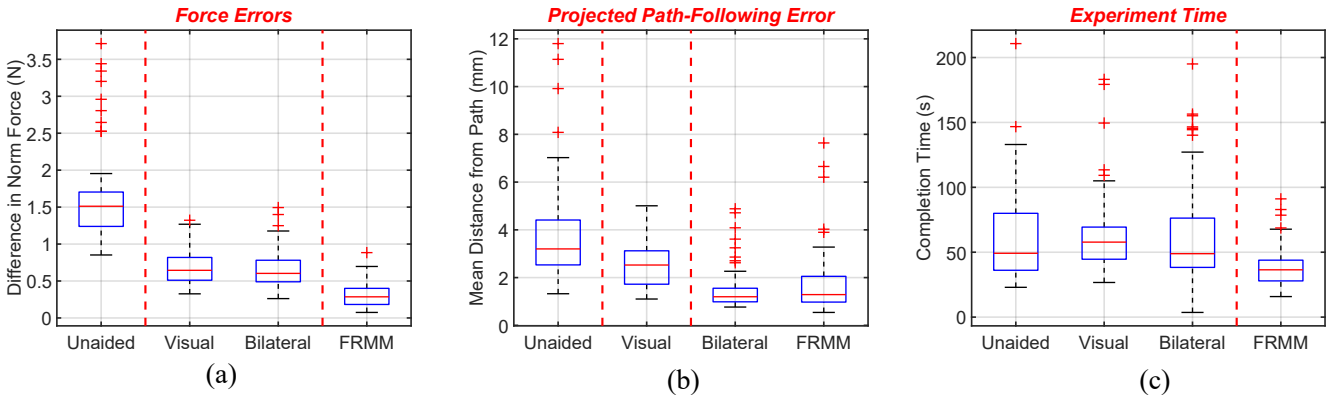

Fig. 7: Boxplots of results in mock ablation tasks - the central red line is the median, with the box covering the 25th to 75h percentiles of the data. Outliers, plotted with a cross, are outside 2.7 standard deviations from the mean, assuming normality. Small dots represent data all the experimental points. Vertical bars separate groups with significantly different means. (A) Force regulation errors (B) Path-following errors (C) Completion time

	Unaided	Visual	Bilateral	FRMM
Path Coverage (%)	97	99	99	100
Force Error (N)	1.63	0.68	0.67	0.30
Path Error (mm)	3.8	2.5	1.5	1.7
Completion Time (s)	60	63	64	38

TABLE IV: Results for ablation experiments. Refer to table II for the definition of user assistance modes and control modes used.

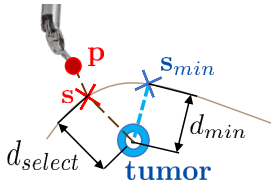

Fig. 8: User-selected locations were determined "close" to a particular mock tumor if d_{select} was within 0.8 mm of d_{min}

In running a Chi-squared test on the datasets, we found that not all the distributions follow the normality assumption from ANOVA and Tukey's test - however, due to the sample size and other empirical results on ANOVA's ability to characterize non-normal datasets [51], we do not believe our statistical conclusions are biased.

The path coverage metric was calculated by cutting the desired path into discrete segments and calculating the closest segment for each position of the robot in contact. The proportion of these segments identified as closest to a point on the robot path characterizes the "coverage". If users frequently lost contact with the organ during task execution, this metric captures those effects. The average coverage for the unassisted mode (97%) was significantly less than the coverage in all the other modes $(p < 0.002)$.

Force regulation errors were calculated as the mean difference between the contact force and the desired regulation force of 3 N. This was only calculated when the user made contact with the organ. This metric had 3 groups of results, shown in Fig. 7a. The unaided results had significantly worse force regulation errors than all other groups with a group mean error of 1.63 N. The results with direct feedback in the Visual and Bilateral modes had lower errors with means of 0.68 N and 0.67 N, respectively. There was no significant difference between these two groups. Outperforming all these results was the FRMM mode with a mean error of 0.30 N, which significantly improved force regulation over all other methods. For all these comparisons, $(p < 0.0001)$.

Path-following errors were calculated by projecting the current robot position into a plane fit to the desired path and calculating the distance between the projected current point to the projected curve points. This separates path-following errors from force errors so that errors in the surface normal direction are not double-counted as both force errors and path-following errors. As shown in Fig. 7b, the final two modes using a PVF significantly improved path-following over the first two modes $(p < 0.004)$. The Visual mode also had reduced errors when compared to the Unaided mode $(p < 0.0001)$.

The completion time, in Fig. 7c, was calculated as the total time required to complete one cycle of ablation (moving from one end of the path and back) and was found to be significantly reduced in FRMM compared to all other modes, $(p < 0.0002)$, which were not significantly different from each other.

B. Organ Palpation

The palpation experiments did not have as many strong differences as the ablation experiments. The metrics for these experiments are shown in Table V. To determine selection accuracy, each point selected by the user as a possible location for a hard "mock tumor" was marked as either being "close to" one of the subsurface features or not. If multiple points were selected close to an actual feature, the closest point was taken as the only accepted point and the other points were designated as additional selected points, not belonging to any feature. As shown in Fig. 8, each tumor had some minimum distance to the surface d_{min}. When a user digitized a point, the closest point to the surface, $\mathbf{s}$, was found and its distance to the center of the tumor was calculated as d_{select}. If $d_{select} - d_{min} < 0.8mm$, the selected point was designated as "close" to that particular tumor. This metric, rather than the pure distance across the surface of the organ from $\mathbf{s_{min}}$ to $\mathbf{s}$, better captured closeness to a tumor on curved surfaces where surface distance may be far, but the location is still "on top" of the tumor.

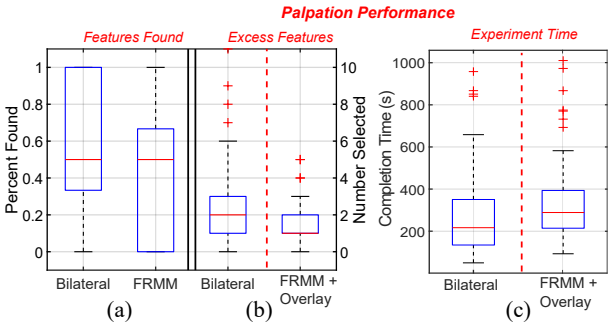

Fig. 9: Percent of features found and excess features found in palpation modes. Refer to Fig. 7 for boxplot formulation.

	Bilateral	FRMM
Excess Features	1.9	1.5
Features Found (%)	54	43
Total Time (s)	268	333

TABLE V: Results of palpation experiments: similar feature-finding accuracy was found for both modes with reduced time using bilateral telemanipulation.

Boxplots of the experimental results are shown in Fig. 9. For both methods, many excess points were found by users - on average 1.9 excess points were selected by users in the bilateral experiments and 1.5 in the FRMM+Overlay experiments, but the distribution had a high variance and this difference had weak statistical significance ($p = 0.0715$). At the same time, many points were missed - on average users only found 54% of the features in an organ in the Bilateral experiments and 43% in the FRMM+Overlay experiments. This result was statistically significant with an α of 0.05 ($p = 0.0235$).

Users were able to complete experiments with haptic feedback in the Bilateral mode more quickly than when using visual feedback with FRMM+Overlay (333 vs. 268 seconds, $p = 0.013$ using a 2-sample t-test).

C. Subjective Results

A questionnaire was given to each user enrolled in the study. A series of questions were asked of each user before, after, and during the experiments. For both tasks, the mode with the most assistance (FRMM) was preferred by a majority of users and users reported significantly reduced effort in that mode.

For the ablation experiments, a majority (69% of users) preferred the FRMM mode, with 7% preferring the Bilateral mode and 27% preferring the Visual mode. No users preferred the Unaided mode. In the palpation task, 84% of users preferred FRMM+Overlay over Bilateral assistance.

After completing each experimental mode, users were asked a series of questions on a scale of 1 to 7 using the NASA/TLX scale evaluating mental/physical effort and difficulty of the task they had just completed where higher scores indicate a demanding task that requires a large amount of focus and difficulty [52]. The results of these questions are charted in Fig. 10. In ablation, the FRMM mode significantly reduced TLX effort scores over all the other groups ($p < 0.006$) with a mean of 9.4 compared to the other modes with mean scores above 14. In the palpation experiments, the FRMM+Overlay mode was also associated with significantly reduced aggregate

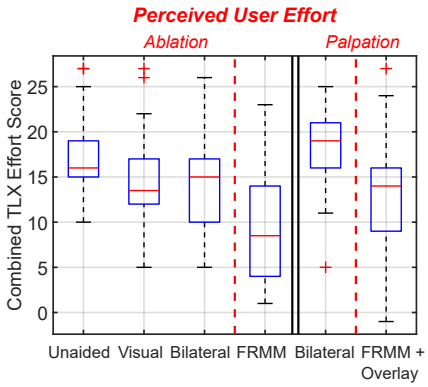

Fig. 10: NASA/TLX scores from users in all experimental conditions: ablation experiments on the left, palpation on the right. Stars indicate a significant difference in mean effort from other modes in that experiment type. Refer to Fig. 7 for boxplot formulation.

TLX effort scores ($p = 0.002$) with a mean score of 13.3 compared to a mean score of 18.3 using haptic feedback.

VI. Discussion

We found that our model-mediated telemanipulation framework with assistance modes greatly increased the ability of the system to regulate positions and forces during a path-following task and led to reduced user effort during palpation.

A. Ablation Task

The reduction in path coverage in the Unaided control mode indicated that users tended to lose contact in that mode when there was no force feedback, as would be expected. As the coverage still had an average of 97%, most users did not lose a very large amount of contact with the path, but the difference still may be important depending on the clinical context.

The difference in quality of contact is more pronounced in force regulation errors. When completely unaided, force regulation errors were much higher than when some form of guidance was added. The Visual and Bilateral modes were indistinguishable, indicating that the addition of kinesthetic feedback in the Bilateral mode was not useful in better force regulation. Since both tasks used visual feedback, that may be sufficient in completing similar tasks. The use of semi-automated force regulation using the FRMM mode allowed further reductions in force regulation errors, showing the utility of shared control for accurate forceful interaction tasks.

In the success of path-following, the Bilateral and FRMM modes both had the least errors due to the use of a PVF pushing the users to follow the path closely. Also, even though no feedback about path-following was introduced between the Unaided and Visual modes, the Visual mode also presented reduced path-following errors over the Unaided mode. It can be hypothesized that the additional contact information helped users reduce mental effort spent on regulating contact forces, allowing them to focus more on the line-following task, reducing path-following errors.

Only the FRMM mode showed a decrease in completion time. While other feedback methods improved performance via some of the other metrics, it appears that either a certain

threshold of assistance is necessary before time can be reduced, or that the force-regulation task is much more complicated and slows users without semi-automated assistance. This result indicates that speed does not have to be compromised in order to improve task-completion performance, as the FRMM mode also improved the other metrics as well. Subjective responses indicated that the majority of users preferred the FRMM mode.

The presence of a subgroup preferring no force feedback suggests that visual feedback may be more useful or intuitive for enabling users to control robot motion and make intelligent decisions regarding interaction forces. It may be instructive to further elucidate exactly how visual perception compares to force feedback, as in this study there was no difference in a users's ability to perform a force-regulation task when force feedback was added in addition to a visual cue.

In this experiment, a constant interaction force was desired throughout the entire experiment. Other control options would need to be presented to the user to adapt this framework to allow for user-controlled changes in the regulation forces by using a footpedal or some other additional input device.

B. Palpation Task

The results from the palpation experiments were more mixed than those of the ablation experiments. Although the semi-automated palpation mode did not show improvement in the identification of subsurface features compared to direct haptic feedback in the Bilateral mode, users preferred more assistance during palpation tasks, suggesting the proposed method's potential utility, pending further development.

We believe there are a number of reasons why palpation was difficult. The long probe grasped by the gripper in order to allow for optical tracking for better ground truth measurement was a challenge in that it extended the lever arm of the wrist, which is somewhat compliant during high-force interaction events. While the OVF assisted users in reducing the effects of this problem, it was likely still a source of reduced efficacy. While users reported that they liked seeing the visual feedback from the overlay, it took a significant amount of time to update the GP with enough data to cover all of the organ at a sufficient level of resolution to find relatively small stiff features. Further, while the GP estimation method carries within it metrics describing uncertainty of estimates, this was not part of the visual feedback to the user - therefore, the GP could change as an interpolated section of the stiffness map was updated by new data from the user.

An issue in the results using direct force feedback of the MTM of the dVRK is that the MTM, while capable of providing force feedback, was not designed to be a high-fidelity haptic device. The utility of future haptic feedback systems using force feedback may be improved by investigating alternative haptic feedback devices that may allow for better user understanding of probe-environment interaction forces than the MTM.

VII. Conclusion and Future Work

We presented a framework for model-mediated telemanipulation and the assessment of various haptic and visual feedback methods for assistance in task completion during forceful interaction with simulated surgical tasks.

In the ablation test, investigating regulation of forces, we showed that our model-mediated control method with visual feedback, semi-autonomous force control, and VF assistance could improve accuracy in path following, reduce errors in force regulation, decrease experiment time, and also reduce users' mental burden. This is a promising result indicating that future research could benefit from using elements of this interaction scheme to improve surgical quality and reduce mental load on surgeons.

In the exploration of palpation, we found that visual feedback provided less stress and more comfort and confidence of users while performing palpation tasks. However, while users preferred the assistive mode, they did not perform better than when using kinesthetic feedback in a standard bilateral telemanipulation architecture.

Future work should include further investigation of palpation methods for improving the ability to find subsurface features in a rapid and accurate manner. Further exploration of semi-automated force regulation should be pursued both for other tasks within minimally invasive surgery and in other environments requiring force regulation during task execution in telemanipulated systems.

VIII. Acknowledgement

The authors wish to thank Colette Abah and Neel Shihora for supporting this work in design assistance for the silicone phantom organs. We also thank Dr. Robert Labadie for providing access to the CT scanner.

This work was supported by a multi-site National Robotics Initiative grants "NRI: Large: Collaborative Research: Complementary Situational Awareness for Human-Robot Partnerships" (NSF NRI IIS 1327566, 1426655, 1327657). The da Vinci Research Kit is supported by "NRI: Collaborative Research: Software Framework for Research in Semi-Autonomous Teleoperation" (NSF NRI IIS 1637789).

References

[1] A. Talasaz, A. L. Trejos, and R. V. Patel, "Effect of force feedback on performance of robotics-assisted suturing," in *Biomedical Robotics and Biomechatronics (BioRob), 2012 4th IEEE RAS & EMBS International Conference on*. IEEE, 2012, pp. 823–828.

[2] M. J. Massimino and T. B. Sheridan, "Sensory substitution for force feedback in teleoperation," *Presence: Teleoperators & Virtual Environments*, vol. 2, no. 4, pp. 344–352, 1993.

[3] B. T. Bethea, A. M. Okamura, M. Kitagawa, T. P. Fitton, S. M. Cattaneo, V. L. Gott, W. A. Baumgartner, and D. D. Yuh, "Application of haptic feedback to robotic surgery," *Journal of Laparoendoscopic & Advanced Surgical Techniques*, vol. 14, no. 3, pp. 191–195, 2004.

[4] C. Pacchierotti, D. Prattichizzo, and K. J. Kuchenbecker, "Cutaneous feedback of fingertip deformation and vibration for palpation in robotic surgery," *IEEE Trans. Biomed. Eng.*, vol. 63, no. 2, pp. 278–287, 2016.

[5] D. Prattichizzo, C. Pacchierotti, S. Cenci, K. Minamizawa, and G. Rosati, "Using a fingertip tactile device to substitute kinesthetic feedback in haptic interaction," in *Proceedings of the 2010 International Conference on Haptics: Generating and Perceiving Tangible Sensations, Part I*, ser. EuroHaptics'10. Berlin, Heidelberg: Springer-Verlag, 2010, pp. 125–130. [Online]. Available: http://dl.acm.org/citation.cfm?id=1884164.1884184

[6] M. Li, J. Konstantinova, G. Xu, B. He, V. Aminzadeh, J. Xie, H. Wurdemann, and K. Althoefer, "Evaluation of stiffness feedback for hard nodule identification on a phantom silicone model," *PloS one*, vol. 12, no. 3, p. e0172703, 2017.

[7] A. Lécuyer, J.-M. Burkhardt, and C.-H. Tan, "A study of the modification of the speed and size of the cursor for simulating pseudo-haptic bumps and holes," *ACM Transactions on Applied Perception (TAP)*, vol. 5, no. 3, p. 14, 2008.

[8] C. R. Wagner, N. Stylopoulos, and R. D. Howe, "The role of force feedback in surgery: analysis of blunt dissection," in *Proceedings 10th Symposium on Haptic Interfaces for Virtual Environment and Teleoperator Systems. HAPTICS 2002*, March 2002, pp. 68–74.

[9] T. Yamamoto, N. Abolhassani, S. Jung, A. M. Okamura, and T. N. Judkins, "Augmented reality and haptic interfaces for robot-assisted surgery," *The International Journal of Medical Robotics and Computer Assisted Surgery*, vol. 8, no. 1, pp. 45–56, 2012.

[10] M. Mahvash, J. Gwilliam, R. Agarwal, B. Vagvolgyi, L.-M. Su, D. D. Yuh, and A. M. Okamura, "Force-feedback surgical teleoperator: Controller design and palpation experiments," in *2008 Symposium on Haptic Interfaces for Virtual Environment and Teleoperator Systems*. IEEE, 2008, pp. 465–471.

[11] L. Meli, C. Pacchierotti, and D. Prattichizzo, "Experimental evaluation of magnified haptic feedback for robot-assisted needle insertion and palpation," *The International Journal of Medical Robotics and Computer Assisted Surgery*, vol. 13, no. 4, p. e1809, 2017.

[12] M. Shahbazi, S. F. Atashzar, and R. V. Patel, "A systematic review of multilateral teleoperation systems," *IEEE Trans. Haptics*, vol. 11, no. 3, pp. 338–356, 2018.

[13] T. Osa, N. Sugita, and M. Mitsuishi, "Online trajectory planning and force control for automation of surgical tasks," *IEEE Trans. Autom. Sci. Eng.*, vol. 15, no. 2, pp. 675–691, 2017.

[14] N. Simaan, R. M. Yasin, and L. Wang, "Medical Technologies and Challenges of Robot-Assisted Minimally Invasive Intervention and Diagnostics," *Annual Review of Control, Robotics, and Autonomous Systems*, vol. 1, no. 1, pp. 465–490, may 2018. [Online]. Available: https://www.annualreviews.org/doi/10.1146/annurev-control-060117-104956

[15] N. Simaan, R. H. Taylor, and H. Choset, "Intelligent surgical robots with situational awareness," *Mechanical Engineering Magazine Select Articles*, vol. 137, no. 09, pp. S3–S6, 2015.

[16] R. A. Srivatsan, E. Ayvali, L. Wang, R. Roy, N. Simaan, and H. Choset, "Complementary model update: A method for simultaneous registration and stiffness mapping in flexible environments," in *Robotics and Automation (ICRA), 2016 IEEE International Conference on*. IEEE, 2016, pp. 924–930.

[17] P. Chalasani, L. Wang, R. Roy, N. Simaan, R. H. Taylor, and M. Kobilarov, "Concurrent nonparametric estimation of organ geometry and tissue stiffness using continuous adaptive palpation," in *2016 IEEE International Conference on Robotics and Automation (ICRA)*, May 2016, pp. 4164–4171.

[18] E. Ayvali, R. A. Srivatsan, L. Wang, R. Roy, N. Simaan, and H. Choset, "Using bayesian optimization to guide probing of a flexible environment for simultaneous registration and stiffness mapping," in *Robotics and Automation (ICRA), 2016 IEEE International Conference on*. IEEE, 2016, pp. 931–936.

[19] L. Wang, Z. Chen, P. Chalasani, R. M. Yasin, P. Kazanzides, R. H. Taylor, and N. Simaan, "Force-controlled exploration for updating virtual fixture geometry in model-mediated telemanipulation," *Journal of Mechanisms and Robotics*, vol. 9, no. 2, p. 021010, 2017.

[20] H. Liu, D. P. Noonan, B. J. Challacombe, P. Dasgupta, L. D. Seneviratne, and K. Althoefer, "Rolling mechanical imaging for tissue abnormality localization during minimally invasive surgery," *IEEE Trans. Biomed. Eng.*, vol. 57, no. 2, pp. 404–414, 2010.

[21] A. Galea and R. Howe, "Tissue stiffness from tactile imaging," in *Engineering in Medicine and Biology, 2002. 24th Annual Conference and the Annual Fall Meeting of the Biomedical Engineering Society EMBS/BMES Conference, 2002. Proceedings of the Second Joint*, vol. 2. IEEE, 2002, pp. 935–936.

[22] S. B. Kesner and R. D. Howe, "Discriminating tissue stiffness with a haptic catheter: Feeling the inside of the beating heart," in *World Haptics Conference (WHC), 2011 IEEE*. IEEE, 2011, pp. 13–18.

[23] V. Egorov, H. Van Raalte, and A. P. Sarvazyan, "Vaginal tactile imaging," *IEEE Trans. Biomed. Eng.*, vol. 57, no. 7, pp. 1736–1744, 2010.

[24] A. P. Miller, W. J. Peine, J. S. Son, and M. Z. T. Hammoud, "Tactile imaging system for localizing lung nodules during video assisted thoracoscopic surgery," in *Proceedings 2007 IEEE International Conference on Robotics and Automation*. IEEE, 2007, pp. 2996–3001.

[25] K. Xu and N. Simaan, "Intrinsic wrench estimation and its performance index for multisegment continuum robots," *IEEE Trans. Robot.*, vol. 26, no. 3, pp. 555–561, 2010.

[26] K. Nichols, A. M. Okamura *et al.*, "Autonomous robotic palpation: Machine learning techniques to identify hard inclusions in soft tissues," in *Robotics and Automation (ICRA), 2013 IEEE International Conference on*. IEEE, 2013, pp. 4384–4389.

[27] S. McKinley, A. Garg, S. Sen, R. Kapadia, A. Murali, K. Nichols, S. Lim, S. Patil, P. Abbeel, A. M. Okamura *et al.*, "A single-use haptic palpation probe for locating subcutaneous blood vessels in robot-assisted minimally invasive surgery," in *2015 IEEE International Conference on Automation Science and Engineering (CASE)*. IEEE, 2015, pp. 1151–1158.

[28] R. E. Goldman, A. Bajo, and N. Simaan, "Algorithms for autonomous exploration and estimation in compliant environments," *Robotica*, vol. 31, no. 1, pp. 71–87, 2013.

[29] N. Haouchine, W. Kuang, S. Cotin, and M. Yip, "Vision-based force feedback estimation for robot-assisted surgery using instrument-constrained biomechanical three-dimensional maps," *IEEE Robotics and Automation Letters*, vol. 3, no. 3, pp. 2160–2165, 2018.

[30] P. Mitra and G. Niemeyer, "Model mediated telemanipulation," in *ASME 2006 International Mechanical Engineering Congress and Exposition*. American Society of Mechanical Engineers, 2006, pp. 1393–1401.

[31] ——, "Model-mediated telemanipulation," *The International Journal of Robotics Research*, vol. 27, no. 2, pp. 253–262, 2008.

[32] X. Li and P. Kazanzides, "Task frame estimation during model-based teleoperation for satellite servicing," in *2016 IEEE International Conference on Robotics and Automation (ICRA)*. IEEE, 2016, pp. 2834–2839.

[33] T. Xia, S. Léonard, I. Kandaswamy, A. Blank, L. L. Whitcomb, and P. Kazanzides, "Model-based telerobotic control with virtual fixtures for satellite servicing tasks," in *Robotics and Automation (ICRA), 2013 IEEE International Conference on*. IEEE, 2013, pp. 1479–1484.

[34] P. Chalasani, A. Deguet, P. Kazanzides, and R. H. Taylor, "A computational framework for complementary situational awareness (csa) in surgical assistant robots," in *2018 Second IEEE International Conference on Robotic Computing (IRC)*. IEEE, 2018, pp. 9–16.

[35] P. Chalasani, L. Wang, R. Yasin, N. Simaan, and R. H. Taylor, "Preliminary evaluation of an online estimation method for organ geometry and tissue stiffness," *IEEE Robotics and Automation Letters*, vol. 3, no. 3, pp. 1816–1823, 2018.

[36] P. Kazanzides, Z. Chen, A. Deguet, G. S. Fischer, R. H. Taylor, and S. DiMaio, "An open-source research kit for the da Vinci® surgical robot," in *IEEE Intl. Conf. on Robotics and Auto. (ICRA)*, May 2014.

[37] Z. Chen, A. Deguet, R. Taylor, S. DiMaio, G. Fischer, and P. Kazanzides, "An open-source hardware and software platform for telesurgical robot research," in *MICCAI Workshop on Systems and Arch. for Computer Assisted Interventions*, Sep 2013.

[38] M. Y. Jung, A. Deguet, and P. Kazanzides, "A component-based architecture for flexible integration of robotic systems," in *Intelligent Robots and Systems (IROS), 2010 IEEE/RSJ International Conference on*. IEEE, 2010, pp. 6107–6112.

[39] H. Lin, C. Vincent Hui, Y. Wang, A. Deguet, P. Kazanzides, and K. W. S. Au, "A reliable gravity compensation control strategy for dvrk robotic arms with nonlinear disturbance forces," *IEEE Robotics and Automation Letters*, vol. 4, no. 4, pp. 3892–3899, Oct 2019.

[40] M. Raibert and J. Craig, "Hybrid position/force control of manipulators1," *Journal of Dynamic Systems, Measurement, and Control*, vol. 102, p. 127, 1981.

[41] R. Featherstone, S. Thiebaut, and O. Khatib, "A general contact model for dynamically decoupled force/motion control," in *IEEE International Conference on Robotics and Automation*, 1999, pp. 10–15.

[42] D. M. Kwartowitz, S. D. Herrell, and R. L. Galloway, "Toward image-guided robotic surgery: determining intrinsic accuracy of the da Vinci robot," *International Journal of Computer Assisted Radiology and Surgery*, vol. 1, no. 3, pp. 157–165, oct 2006. [Online]. Available: http://link.springer.com/10.1007/s11548-006-0047-3

[43] ——, "Update: Toward image-guided robotic surgery: determining the intrinsic accuracy of the daVinci-S robot," *International Journal of Computer Assisted Radiology and Surgery*, vol. 1, no. 5, pp. 301–304, mar 2007. [Online]. Available: http://link.springer.com/10.1007/s11548-006-0064-2

[44] P. Puangmali, K. Althoefer, L. D. Seneviratne, D. Murphy, and P. Dasgupta, "State-of-the-art in force and tactile sensing for minimally invasive surgery," *IEEE Sensors J.*, vol. 8, no. 4, pp. 371–381, 2008.

[45] A. Trejos, R. Patel, and M. Naish, "Force sensing and its application in minimally invasive surgery and therapy: a survey," *Proceedings of the Institution of Mechanical Engineers, Part C: Journal of Mechanical Engineering Science*, vol. 224, no. 7, pp. 1435–1454, 2010.

[46] A. Fedorov, R. Beichel, J. Kalpathy-Cramer, J. Finet, J.-C. Fillion-Robin, S. Pujol, C. Bauer, D. Jennings, F. Fennessy, M. Sonka *et al.*, "3d slicer as an image computing platform for the quantitative imaging network," *Magnetic resonance imaging*, vol. 30, no. 9, pp. 1323–1341, 2012.

[47] J. M. Fitzpatrick, J. B. West, and C. R. Maurer, "Predicting error in rigid-body point-based registration," *IEEE Trans. Med. Imag.*, vol. 17, no. 5, pp. 694–702, 1998.
[48] A. Myronenko and X. Song, "Point set registration: coherent point drift." *IEEE Trans. Pattern Anal. Mach. Intell.*, vol. 32, no. 12, pp. 2262–75, Dec. 2010.
[49] R. Yasin, L. Wang, C. Abah, and N. Simaan, "Using continuum robots for force-controlled semi autonomous organ exploration and registration," in *Medical Robotics (ISMR), 2018 International Symposium on*. IEEE, 2018, pp. 1–6.
[50] S. Umeyama, "Least-squares estimation of transformation parameters between two point patterns," *IEEE Trans. Pattern Anal. Mach. Intell.*, no. 4, pp. 376–380, 1991.
[51] M. J. Blanca, R. Alarcón, J. Arnau, R. Bono, and R. Bendayan, "Non-normal data: Is anova still a valid option?" *Psicothema*, vol. 29, no. 4, pp. 552–557, 2017.
[52] S. G. Hart, "Nasa-task load index (nasa-tlx); 20 years later," in *Proceedings of the human factors and ergonomics society annual meeting*, vol. 50, no. 9. Sage publications Sage CA: Los Angeles, CA, 2006, pp. 904–908.

Rashid Yasin received the B.S. degree in engineering sciences from Harvard University, Cambridge, MA, USA, in 2012, and the M.S. degree in mechanical engineering from the University of California, Los Angeles, CA, USA, in 2014. He completed the Ph.D. degree at Vanderbilt University, Nashville, TN, USA in 2020. His research interests include medical robotics, medical device development, mechatronics, and control systems.

Preetham Chalasani completed the B. Tech. degree in Information Technology from the Indian Institute of Information Technology in 2012 and the M.S. degree in Computer Science from Johns Hopkins University, Baltimore M.D in 2012. He received his Ph.D. degree in Computer Science from Johns Hopkins in 2018.

Nicolas Zevallos is Artist in Residence at Carnegie Mellon University in Pittsburgh, PA. He specializes in augmented reality for surgical robotics.

Mahya Shahbazi is a Postdoctoral Fellow at the Laboratory for Computational Sensing and Robotics (LCSR), Johns Hopkins University, Baltimore, Maryland, USA. She received her Ph.D. degree in Electrical and Computer Engineering from the University of Western Ontario, London, ON, Canada, in 2017. Mahya was a visiting research scholar at the University of Alberta, Canada, in 2014, and a Postdoctoral Associate at Canadian Surgical Technologies and Advanced Robotics (CSTAR) Centre in 2017-2018. She has been recipient of several prestigious awards including the 2014 Ontario Graduate Scholarship and the 2018-2019 NSERC Postdoctoral Fellowship. Her main research interests include Medical Robotics, Haptics and Teleoperation, Human-Robot Interaction, Advanced Control Systems, and Artificial Intelligence.

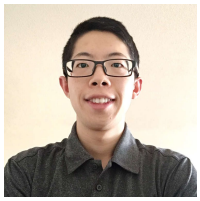

Zhaoshuo Li received his BASc in Mechatronics Engineering (honors) from University of British Columbia, Vancouver, Canada, in 2018. He is currently working towards a PhD in Computer Science at Johns Hopkins University, Baltimore, US. His research interest includes computer vision and virtual fixture for medical robotics and image-guided interventions.

Anton Deguet received the B.S. degree in mathematics in 1991 from the University of Tours, Tours, France, and the M.S. degree in computer science in 1994 from the University of Grenoble, Grenoble, France. Since 2000, he has been a research systems engineer with the Center for Computer Integrated Surgery, The Johns Hopkins University, Baltimore, MD.

Peter Kazanzides received the Ph.D. degree in electrical engineering from Brown University in 1988 and began work on surgical robotics as a postdoctoral researcher at the IBM T.J. Watson Research Center. He co-founded Integrated Surgical Systems (ISS) in November 1990 to develop the ROBODOC System, which has been used for more than 20,000 hip and knee replacement surgeries. Dr. Kazanzides joined Johns Hopkins University in 2002, where he is appointed as a Research Professor of Computer Science. His current research is in the areas of medical robotics, space robotics and augmented reality. In addition, he develops and supports open research platforms such as the da Vinci Research Kit (dVRK).

Howie Choset Howie Choset (F15) received the B.S.Eng. degree in computer science, and the B.S.Econ degree in entrepreneurial management from University of Pennsylvania (Wharton), PA, USA, in 1990, the M.S. and Ph.D. degrees in mechanical engineering from California Institute of Technology (Caltech), CA, USA, in 1991 and 1996, respectively. He is a Professor of robotics with Carnegie Mellon University, Pittsburgh, PA, USA. His research group reduces complicated high-dimensional problems found in robotics to low-dimensional simpler ones for design, analysis, and planning. He directs the Undergraduate Robotics Major at Carnegie Mellon and teaches an overview course on robotics, which uses series of custom developed Lego Labs to complement the course work. He has authored a book entitled Principles of Robot Motion (MIT Press, 2015). Prof. Choset was elected as one of the top 100 innovators in the world under 35, by the MIT Technology Review, in 2002. In 2014, Popular Science selected his medical robotics work as the Best of Whats New in Health Care.

Russell H. Taylor has over 30 years' experience in medical robotics and over 40 in robotics research. He received his Ph.D. in Computer Science from Stanford in 1976. After spending 1976 to 1995 as a Research Staff Member and research manager at IBM Research, he moved to Johns Hopkins University in 1995, where he is the John C. Malone Professor of Computer Science with joint appointments in Mechanical Engineering, Radiology, and Surgery and Director of the of the Laboratory for Computational Sensing and Robotics (LCSR). He is the author of over 450 peer-reviewed journal and conference publications and 80 patents and has received numerous awards and honors.

Nabil Simaan (SM'13) received his Ph.D. degree in mechanical engineering from the Technion—Israel Institute of Technology, Haifa, Israel, in 2002. After a postdoc at Johns Hopkins University National Science Foundation (NSF) Engineering Research Center for Computer-Integrated Surgical Systems and Technology (ERC-CISST) he joined Columbia University in 2005 as an Assistant Professor. In 2009 he received the NSF Career award for young investigators to design new algorithms and robots for safe interaction with the anatomy. In Fall 2010 he joined Vanderbilt University as an Associate Professor, Nashville, TN. His research interests include medical robotics, continuum robots, parallel mechanisms, human-robot physical interaction.